Acta Crystallographica Section A
Foundations of Crystallography
ISSN 0108-7673

Received 8 June 2010
Accepted 19 August 2010

X-ray diffraction peaks from correlated dislocations: Monte Carlo study of dislocation screening

Vladimir M. Kaganer[a]* and Karl K. Sabelfeld[b]

[a]Paul-Drude-Institut für Festkörperelektronik, Hausvogteiplatz 5–7, 10117 Berlin, Germany, and [b]Institute of Computational Mathematics and Mathematical Geophysics, Russian Academy of Sciences, Lavrentiev Prospect 6, 630090 Novosibirsk, Russia. Correspondence e-mail: kaganer@pdi-berlin.de

X-ray diffraction peak profiles are calculated by the Monte Carlo method for arbitrarily correlated dislocations without making any approximations or simplifications. The arrangement of dislocations in pairs with opposite Burgers vectors provides screening of the long-range strains. Moreover, any screening can be modeled by appropriate distribution of the dislocation pairs. Analytical description of the peak profiles is compared with the Monte Carlo results. Symmetric peaks due to screw dislocations and asymmetric peaks due to edge dislocations are simulated and analyzed.

1. Introduction

The broadening of X-ray diffraction peaks due to dislocation displacement fields is a well established tool for studying dislocated crystals. Since X-ray diffraction is sensitive to the total displacements caused by all dislocations, the dislocation density determination from the Bragg peak widths requires the dislocation correlations to be accounted for. Krivoglaz & Ryboshapka (1963) have shown in their seminal paper that the shape of the X-ray diffraction peaks in a crystal containing positionally uncorrelated straight dislocations is described by the Fourier transform of the correlation function

$$G(r) = \exp[-\rho r^2 \ln(R/r)]. \quad (1)$$

Here $r = |\mathbf{r}|$ is a distance in the plane normal to the dislocation lines ($\mathbf{r}$ is a two-dimensional radius vector), ρ is the dislocation density and R is the sample size. We skip here, for the purpose of a qualitative discussion, some factors that are of the order of unity. They are restored in the detailed calculations below.

Equation (1) predicts that the diffraction peak width increases with an increased sample size and diverges for an infinite sample. Krivoglaz & Ryboshapka (1963) argued that the divergence is very slow (logarithmic) and the peak width remains finite for any reasonable size. Later on, Wilkens (1969, 1970*a*,*b*) pointed out that the elastic energy of a crystal with dislocations diverges in just the same way as the correlation function (1). He proposed a 'restrictedly random' dislocation distribution, such that the dislocations arrange in blocks and restrict their total strain field to within the block. The correlation function derived for the restrictedly random dislocation distribution (Wilkens, 1970*a*,*b*) retains the functional form (1), where R becomes the block size. Then, both the elastic energy and the correlation function (1) remain finite. Wilkens (1970*a*) proposed to characterize the block size by a dimensionless parameter $M = R/r_d$, where $r_d = \rho^{-1/2}$ is the mean distance between dislocations. The fits of the experimental peak profiles by equation (1) for such diverse polycrystalline materials as copper, sodium chloride and silicon nitride (Wilkens, 1976; Ungar *et al.*, 1984, 1989, 2001), as well as for threading dislocations in gallium nitride epitaxial films (Kaganer *et al.*, 2005), give values of the parameter M in a range from 1 to 3, thus pointing to a strong screening of a dislocation strain field by just the neighboring dislocations.

Levine & Thomson (1997) and Kamminga & Delhez (2000) used the Monte Carlo method to model the Wilkens restrictedly random dislocation distribution. In both works, several hundreds of uncorrelated parallel dislocations (with equal numbers of dislocations having opposite Burgers vectors) were placed at random in a cylinder of radius R. The calculated diffraction peak profile (Levine & Thomson, 1997) or the correlation function $G(r)$ (Kamminga & Delhez, 2000) obtained from such a dislocation distribution were averaged over a large number of independent samplings, keeping constant the cylinder radius and number of dislocations. Such a model corresponds to grains in a polycrystal, with the grain size R large compared with the mean distance between dislocations r_d. The grain boundaries restrict strain fields of the dislocations within the grain, so that the dislocations of surrounding grains do not need to be included in the calculation. This model corresponds to values of the Wilkens parameter $M > 10$. The distinction between the block size in the Wilkens model and the sample size in the Krivoglaz & Ryaboshapka treatment becomes subtle. On the other hand, the analysis of the experimental peak profiles mentioned above leads to notably smaller values of M, from 1 to 3. If a corresponding block with just a few dislocations is considered,

one can hardly assume that the dislocation strain field does not penetrate to the neighboring blocks.

The initial Wilkens idea that the dislocations rearrange to minimize the total elastic strain has been supported by Zaiser *et al.* (2001) and Csikor & Groma (2004), who modeled the process of elastic relaxation in a system of initially uncorrelated dislocations. They found that dislocations of opposite sign tend to form pairs, while dislocations of the same sign tend to form walls. The exponential distribution of the distances in the dislocation pairs has been found, with the mean distance between dislocations in the pair comparable with the average dislocation separation. The strain field of a dislocation pair is not restricted to within a block. The strain fields of the dislocation pairs overlap.

We show in the present paper that the arrangement of the dislocations of opposite sign in pairs gives rise to a strain field screening that provides the correlation function (1) with a cutoff distance R much smaller than the sample size. Moreover, any screening leading to (1) can be modeled by the dislocation pairs with the appropriate distribution of distances between dislocations in the pair. The cutoff distance R is comparable with the mean separation between dislocations in the pair and can be of the same order or larger than the average distance between dislocations in the sample r_d. We avoid calling these pairs dipoles, since the dislocation dipole is usually considered as a pair with the distance between dislocations much smaller than the distance between dipoles. Theoretical analysis of the X-ray diffraction from dislocation dipoles (Pototskaya & Ryboshapka, 1968; Krivoglaz, 1996) is not applicable in our case, because of the overlapping dislocation pairs.

We calculate in the present paper, using the Monte Carlo method, diffraction peak profiles for distributions of screw and edge dislocations with different types of correlations. Recently we have shown, in an example of diffraction peak profiles from misfit dislocations in epitaxial films, that the Monte Carlo method can be successfully applied to any dislocation distribution with arbitrary predefined positional correlations (Kaganer *et al.*, 2009; Kaganer & Sabelfeld, 2009). Once the positional correlations between dislocations are given, the Monte Carlo calculations do not require any further approximations or simplifications. The diffraction peak profiles thus obtained can be used instead of experimental data to test the approximate analytical formulas. An advantage is full control over all statistical parameters of the dislocation distribution. We compare the Monte Carlo results with equation (1) and its generalizations. The pairs of screw dislocations give rise to symmetric peaks. The pairs of edge dislocations provide asymmetric peaks if pairs of either vacancy or interstitial type dominate.

2. Theory

2.1. Intensity and correlation function

The kinematical X-ray diffraction intensity in the vicinity of a reciprocal-lattice point $\mathbf{Q}$ from a crystal distorted by displacement fields of the defects is given by the product

$$I(\mathbf{q}) = |F_{\mathbf{Q}}|^2 S(\mathbf{q}), \tag{2}$$

where the complex structure amplitude $F_{\mathbf{Q}}$ describes scattering from the average unit cell and the real-valued structure factor $S(\mathbf{q})$ is due to a disorder of the unit cells on distances much larger than the unit-cell size. Here $\mathbf{q}$ is a small deviation from the reciprocal-lattice vector $\mathbf{Q}$. If disorder is absent, the structure factor $S(\mathbf{q})$ reduces to a delta function $\delta(\mathbf{q})$ describing (in the kinematical approximation) the sharp Bragg peaks of an ideal infinite crystal. The crystal lattice defects may reduce intensities of Bragg reflections, shift the Bragg peaks to $\mathbf{q} \neq 0$ and cause diffuse scattering around them (Krivoglaz, 1996).

The structure factor for a crystal distorted by strain fields of defects is given by the Fourier integral

$$S(\mathbf{q}) = \int G(\mathbf{r}) \exp(i\mathbf{q}\cdot\mathbf{r})\, \mathrm{d}\mathbf{r} \tag{3}$$

of the pair correlation function

$$G(\mathbf{r}) = \left\langle \exp\left\{ i[\mathbf{Q}\cdot\mathbf{U}(\mathbf{r}_1) - \mathbf{Q}\cdot\mathbf{U}(\mathbf{r}_2)] \right\} \right\rangle. \tag{4}$$

We consider here translationally invariant systems, so that the correlations depend only on the distance between two points $\mathbf{r} = \mathbf{r}_1 - \mathbf{r}_2$. The total displacement field caused at the point $\mathbf{r}$ by all defects is equal to $\mathbf{U}(\mathbf{r})$. The angular brackets $\langle \ldots \rangle$ in (4) denote the statistical average over the whole ensemble of defects. The structure factor (3) contains both the coherent and diffuse parts. In an ideal crystal, $\mathbf{U}(\mathbf{r}) \equiv 0$, it reduces to a delta function, $S(\mathbf{q}) = (2\pi)^3 \delta(\mathbf{q})$. Writing (3) as a continuous integral rather than a discrete sum over all atoms, we restrict ourselves to the vicinity of a reciprocal-lattice point $\mathbf{Q}$. In other words, the wavevectors $|\mathbf{q}|$ are small compared with $|\mathbf{Q}|$. Then, the defects are described by their elastic displacement fields. Atomic structures of the defects, in particular dislocation cores, are not considered. They are needed to study intensity distributions in wide ranges of wavevectors, from one reciprocal-lattice point to the other.

The formulas in this section are quite general and can be applied to a crystal containing arbitrary defect distributions. Point defects (impurities, clusters, dislocation loops), line defects (dislocations) and planar defects (stacking faults, twins) can be considered simultaneously. They are treated as different defect types. Dislocations with different Burgers vectors, in particular with the opposite Burgers vectors, are considered as different defect types as well. We denote by $\mathbf{u}_\alpha(\mathbf{r} - \boldsymbol{\xi}_{\alpha j})$ the displacement field at the point $\mathbf{r}$ due to a defect of type α located at the position $\boldsymbol{\xi}_{\alpha j}$. Point defects are specified by three-dimensional vectors $\boldsymbol{\xi}_{\alpha j}$ of defect center positions, straight dislocations are specified by two-dimensional vectors in a plane perpendicular to the dislocation lines, and planar defects are specified by the coordinate along a line normal to the defect plane. The integrals over $\boldsymbol{\xi}$ below imply three-, two- or one-dimensional integration, respectively. The total displacement is equal, due to linear elasticity, to the sum of displacements from individual defects,

$$\mathbf{U}(\mathbf{r}) = \sum_{\alpha,j} \mathbf{u}_\alpha(\mathbf{r} - \boldsymbol{\xi}_{\alpha j}). \tag{5}$$

The statistical average (4) is the average over random defect positions $\boldsymbol{\xi}_{\alpha j}$ for each defect type, which was performed by Krivoglaz *et al.* (Krivoglaz, 1961, 1996; Krivoglaz *et al.*, 1983); a brief outline of the derivation was also discussed by Kaganer *et al.* (1997). The correlation function (4) can be represented as

$$G(\mathbf{r}) = \exp[T(\mathbf{r})], \tag{6}$$

where the exponent $T(\mathbf{r})$ is a result of the cumulant expansion over single defects, their pairs, triplets and so on. Accounting for pair correlations is sufficient for most practical applications, so that we write $T(\mathbf{r}) = T_1(\mathbf{r}) + T_2(\mathbf{r})$, where the first term describes the contribution from single defects and the second from their pair correlations. The first term is

$$T_1(\mathbf{r}) = \sum_\alpha \rho_\alpha \int \Phi_\alpha(\mathbf{r}, \boldsymbol{\xi})\, \mathrm{d}\boldsymbol{\xi}, \tag{7}$$

where ρ_α is the density of defects of type α. The term $\Phi_\alpha(\mathbf{r}, \boldsymbol{\xi})$ is defined as

$$\Phi_\alpha(\mathbf{r}_1 - \mathbf{r}_2, \boldsymbol{\xi}) = \exp\{i[\mathbf{Q}\cdot\mathbf{u}_\alpha(\mathbf{r}_1 - \boldsymbol{\xi}) - \mathbf{Q}\cdot\mathbf{u}_\alpha(\mathbf{r}_2 - \boldsymbol{\xi})]\} - 1. \tag{8}$$

The pair-correlations term is

$$T_2(\mathbf{r}) = (1/2)\sum_{\alpha\alpha'} \rho_\alpha\rho_{\alpha'} \times \int \Phi_\alpha(\mathbf{r}, \boldsymbol{\xi})\Phi_{\alpha'}(\mathbf{r}, \boldsymbol{\xi}')C_{\alpha\alpha'}(\boldsymbol{\xi} - \boldsymbol{\xi}')\, \mathrm{d}\boldsymbol{\xi}\, \mathrm{d}\boldsymbol{\xi}', \tag{9}$$

where $C_{\alpha\alpha'}(\boldsymbol{\xi})$ is a pair correlation function for dislocation positions. We consider here, as above, spatially homogeneous systems.

Dislocations are linear defects. We consider in this paper arrays of straight dislocations parallel to each other. Their positions can be represented by two-dimensional vectors $\boldsymbol{\xi}$ in a plane perpendicular to the dislocation lines. Let the z axis be along the dislocation lines. Then, the dislocation displacement field $\mathbf{u}(x, y)$ depends on the coordinates x, y in the plane perpendicular to the dislocation lines. Since the dislocation displacements and hence the correlation function (4) do not depend on z, the structure factor is

$$S(\mathbf{q}) = \delta(q_z)\int G(x, y)\exp(iq_x x + iq_y y)\, \mathrm{d}x\, \mathrm{d}y. \tag{10}$$

The diffracted intensity concentrates in a disc in the reciprocal space in the plane perpendicular to the dislocation lines.

The three-dimensional intensity distribution (10) is usually not measured in a diffraction experiment. In a powder diffraction experiment the average over particle orientations is equivalent to integration of (10) over two components of the vector $\mathbf{q}$ in the plane perpendicular to the reciprocal-lattice vector $\mathbf{Q}$ (Warren, 1969). It reduces (10) to a one-dimensional Fourier integral,

$$S(q) = \int G(x, y = 0)\exp(iqx)\, \mathrm{d}x, \tag{11}$$

where the x axis is chosen so that the reciprocal-lattice vector $\mathbf{Q}$ lies in the (x, z) plane. Very similarly, when a single crystal is studied in a double-crystal diffraction experiment, a wide-open detector accepts the scattered waves of all directions around the direction of the diffracted beam. The integration is performed over the plane perpendicular to the diffracted beam. The scattered intensity is again described by (11), where the x axis is now taken so that the diffracted beam lies in the (x, z) plane (Kaganer *et al.*, 2005). We therefore concentrate in further analysis on the one-dimensional Fourier integral (11). Since the main effort is in the calculation of the correlation function $G(x, y)$, the generalization to a two-dimensional Fourier integral (10) is straightforward.

The limiting value $2W = -\lim_{\mathbf{r}\to\infty} \mathrm{Re}\, T(\mathbf{r})$ controls the presence or absence of the coherent Bragg peak in the scattering intensity (Krivoglaz, 1961, 1996). If W is finite, the diffracted intensity contains the coherent contribution proportional to $\exp(-2W)\delta(\mathbf{q})$, and if W is infinite, the coherent peak is absent. Both uncorrelated dislocations (Krivoglaz & Ryboshapka, 1963) and dislocation dipoles (Pototskaya & Ryboshapka, 1968) result in divergence of M, but the laws are different. Let us discuss them now, since both uncorrelated and correlated dislocations will be considered below. In the limit $\mathbf{r} \to \infty$, the displacements at the points $\mathbf{r}_1$ and $\mathbf{r}_2$ in (4) are not correlated and equation (7) gives

$$W = \sum_\alpha \rho_\alpha \int \left\{1 - \cos[\mathbf{Q}\cdot\mathbf{u}_\alpha(\boldsymbol{\xi})]\right\} \mathrm{d}\boldsymbol{\xi}. \tag{12}$$

The displacement field of a dislocation does not decay with the distance from the dislocation, and the integral (12) diverges proportionally to the system size L. The displacement field of a dislocation dipole decays, on distances much larger than the dipole width, as $1/\xi$, and the two-dimensional integral (12) contains a factor $\int \mathrm{d}\xi/\xi$, where the integration is performed from the dipole width D to the system size L. Therefore, $W \propto \ln(L/D)$ is finite in a finite sample but logarithmically diverges with increasing its size. In the analysis of the peak shapes below, we assume that the sample is large enough and do not consider the coherent contribution. The diffraction peaks analyzed below can be considered as diffuse peaks, in the sense that the structure factor $S(\mathbf{q})$ does not contain a singularity.

2.2. Screening due to dislocation correlations

The aim of this section is to find minimum requirements for dislocation correlations that provide screening of the long-range strain fields, so that the length R in (1) does not depend on the sample size. Wilkens' restrictedly random distribution is one possible realization of screening. Krivoglaz *et al.* (1983) considered several correlation functions for dislocation positions, assuming the same correlations for dislocations of the same sign and those of opposite signs. We follow the line of their analysis but allow different correlations.

The integral (7) collects contributions from all dislocations uniformly distributed over the plane $\boldsymbol{\xi}$. The calculation below will show that the main contribution to the integral comes from the far dislocations, whose distance from the origin $\xi = |\boldsymbol{\xi}|$ is large compared with the distance $r = |\mathbf{r_1} - \mathbf{r_2}|$ between the points where the correlations are sought. Then, the difference of displacements can be expanded in a Taylor series to the first order,

$$\mathbf{Q}\cdot\mathbf{u}_\alpha(\mathbf{r}_1-\xi)-\mathbf{Q}\cdot\mathbf{u}_\alpha(\mathbf{r}_2-\xi)\approx r_k Q_l w_{\alpha kl}=gb(r/\xi)\Psi_\alpha, \tag{13}$$

where r_k are the Cartesian coordinates of the vector $\mathbf{r}$, summation over repeated indices is implied, and $\Psi_\alpha = \Psi_\alpha(\hat{\mathbf{Q}},\hat{\mathbf{b}},\hat{\mathbf{r}},\hat{\boldsymbol{\xi}})$ is an angular factor of the order of 1 that depends on the directions of all vectors involved in the problem: scattering vector $\hat{\mathbf{Q}}$, Burgers vector $\hat{\mathbf{b}}$, correlation distance $\hat{\mathbf{r}}$ and dislocation position $\hat{\boldsymbol{\xi}}$. The $1/\xi$ decay of distortions is a general property of the dislocation elastic fields. The factor $gb = Qb/2\pi$ is proportional to the reflection order. Elastic distortions due to defects of type α are defined as

$$w_{\alpha kl}(\boldsymbol{\xi})=\partial u_{\alpha l}/\partial\xi_k. \tag{14}$$

The approximation (13) makes sense for $\xi \gg r$. If a more restrictive condition $\xi \gg gbr$ is satisfied, the exponential function in (8) can be expanded in series, since $\Psi \simeq 1$. The first-order term in the expansion is imaginary. It originates from (7), is linear in $w_{\alpha kl}$ and can be written as

$$\mathrm{Im}\,T_1(\mathbf{r})=r_k Q_l \overline{w}_{kl}, \tag{15}$$

where the mean distortions tensor $\overline{w}_{kl}$ is the result of the average of the dislocation distortions,

$$\overline{w}_{kl}=\sum_\alpha \rho_\alpha \int w_{\alpha kl}(\boldsymbol{\xi})\,\mathrm{d}\boldsymbol{\xi}. \tag{16}$$

The term $\mathrm{Im}\,T_1(\mathbf{r})$ is linear in $\mathbf{r}$ and describes, on the Fourier transformation (3), the shift of the Bragg peak due to mean distortions.

The second-order term of the integral (7) contributes to the real part of $T_1(\mathbf{r})$,

$$\mathrm{Re}\,T_1(\mathbf{r})=-(1/2)\sum_\alpha \rho_\alpha \int\left[gb(r/\xi)\Psi_\alpha\right]^2\mathrm{d}\boldsymbol{\xi}. \tag{17}$$

The integral can be calculated in polar coordinates, $\boldsymbol{\xi}=(\xi,\phi)$,

$$\mathrm{Re}\,T_1(\mathbf{r})=-(1/2)\chi(gb)^2\rho r^2\int \mathrm{d}\xi/\xi, \tag{18}$$

where the factor χ is the result of the angular integration

$$\chi=\sum_\alpha(\rho_\alpha/\rho)\int_0^{2\pi}\Psi_\alpha^2\,\mathrm{d}\phi, \tag{19}$$

and $\rho=\sum_\alpha \rho_\alpha$ is the total dislocation density. The ratio ρ_α/ρ is the fraction of dislocations of the type α. The factor χ defined by (19), also called 'the contrast factor', is a well defined quantity whose proper value is needed for the accurate dislocation density determination. It was calculated for different crystal symmetries, anisotropies and dislocation arrangements in a number of papers. We refer to the most recent publication (Martinez-Garcia *et al.*, 2009) that also reviews previous works. Below we give simple expressions for χ in the dislocation configurations that we study.

The radial integral in (18) diverges at both $\xi\to 0$ and $\xi\to\infty$. It has to be calculated with the lower limit of the order of gbr, which is the applicability limit of the expansion leading to (17), and the upper limit of the order of the sample size L. Finally we obtain

$$\mathrm{Re}\,T_1(\mathbf{r})=-(1/2)\chi(gb)^2\rho r^2\ln(\varsigma' L/gbr), \tag{20}$$

where $\varsigma'\simeq 1$ is a constant factor. This form of the correlation function for uncorrelated dislocations was obtained by Krivoglaz & Ryboshapka (1963).

Let us estimate now the contribution to the integral (7) from the region $\xi \le gbr$, which we excluded above. Since $|\Phi|$ is always less than 2, the contribution to the integral does not exceed $2\pi(gb)^2\rho r^2$. This contribution is negligible if the logarithmic term in (20) is much larger than unity. Krivoglaz & Ryboshapka (1963) concluded that the applicability of the approximation (20) requires not only the sample size L to be large compared with the mean distance between dislocations $r_\mathrm{d}=\rho^{-1/2}$, but its logarithm to be large: $\ln(L/r_\mathrm{d})\gg 1$. One may expect, however, that the applicability of (20) is broader. In the region $\xi \le gbr$, the argument of the exponential function in (8) is large and strongly varies as a function of $\boldsymbol{\xi}$, so that the exponent is averaged to zero on the integration (7). Then, the contribution of this region to the correlation function (20) can be estimated as $-\pi(gb)^2\rho r^2$. Its addition will not change the functional form of the expression (20), but only the parameter L in it. Since L is an experimentally ill-defined quantity, the use of it as a free parameter allows the formula (20) to be applied in a broader range than the one limited by its applicability restriction. The same arguments can be used for the correlation term below.

Let us proceed to the evaluation of the second-order term (9). Using (13) in the same approximations as above, we obtain

$$\mathrm{Re}\,T_2(\mathbf{r})=-(1/2)\sum_{\alpha,\alpha'}\rho_\alpha\rho_{\alpha'}(gb)^2r^2 \times\int\frac{\Psi_\alpha(\hat{\boldsymbol{\xi}})\Psi_{\alpha'}(\hat{\boldsymbol{\xi}}')}{\xi\xi'}C_{\alpha\alpha'}(\boldsymbol{\xi}-\boldsymbol{\xi}')\,\mathrm{d}\boldsymbol{\xi}\,\mathrm{d}\boldsymbol{\xi}'. \tag{21}$$

We expect that the dislocations are decorrelated on large distances, so that the correlation functions $C_{\alpha\alpha'}(\boldsymbol{\xi})$ tend to zero as ξ exceeds some correlation length R_c. The correlation length is small compared with the sample size L. Hence, the integration range in (21) is limited by $|\boldsymbol{\xi}-\boldsymbol{\xi}'|\lesssim R_\mathrm{c}$, while the main contribution to the integral comes from $\xi\gg R_\mathrm{c}$ for the same reasons as above. Since the distance $|\boldsymbol{\xi}-\boldsymbol{\xi}'|$ is small compared with ξ, we can approximate $\xi\xi'$ in the denominator by ξ^2 and replace $\Psi_{\alpha'}(\hat{\boldsymbol{\xi}}')$ with $\Psi_{\alpha'}(\hat{\boldsymbol{\xi}})$. Then, we obtain a product of three separate integrals,

$$\mathrm{Re}\,T_2(\mathbf{r})=-(1/2)\sum_{\alpha,\alpha'}\rho_\alpha\rho_{\alpha'}(gb)^2r^2 \times\int_0^{2\pi}\Psi_\alpha\Psi_{\alpha'}\,\mathrm{d}\phi\int C_{\alpha\alpha'}(\boldsymbol{\xi}')\,\mathrm{d}\boldsymbol{\xi}'\int\mathrm{d}\xi/\xi. \tag{22}$$

The integration over ξ in (22) is performed from a distance of the order of R_c to a distance of the order of L. The resulting term is $\ln(\varsigma'' L/R_\mathrm{c})$, where $\varsigma''\simeq 1$ is a constant.

Let us consider dislocations with opposite Burgers vectors. Their angular factors Ψ_+ and Ψ_- have opposite values, $\Psi_+ = -\Psi_-$. Then, (22) becomes

$$\begin{aligned}\mathrm{Re}\, T_2(\mathbf{r}) = & -(1/2)\chi(gb)^2 r^2 \ln(\varsigma'' L/R_\mathrm{c}) \\ & \times \int \left[\rho_+^2 C_{++}(\boldsymbol{\xi}) + \rho_-^2 C_{--}(\boldsymbol{\xi}) \right. \\ & \left. - 2\rho_+\rho_- C_\pm(\boldsymbol{\xi})\right] \mathrm{d}\boldsymbol{\xi}. \end{aligned} \quad (23)$$

We can now formulate the general condition for the screening of the dislocation strain fields: the sum of the first-order term (20) and the second-order term (23) does not depend on the sample size L if the following condition is satisfied,

$$\int \left[\rho_+^2 C_{++}(\boldsymbol{\xi}) + \rho_-^2 C_{--}(\boldsymbol{\xi}) - 2\rho_+\rho_- C_\pm(\boldsymbol{\xi})\right] \mathrm{d}\boldsymbol{\xi} + \rho = 0. \quad (24)$$

Then, the real part of the correlation function $T(\mathbf{r}) = T_1(\mathbf{r}) + T_2(\mathbf{r})$ is given by

$$\mathrm{Re}\, T(\mathbf{r}) = -(1/2)\chi(gb)^2 \rho r^2 \ln(\varsigma R_\mathrm{c}/gbr), \quad (25)$$

and does not depend on the sample size L. Here $\varsigma = \varsigma'/\varsigma'' \simeq 1$ is a constant.

The condition (24) can be satisfied by various kinds of dislocation distributions. For example, if $C_\pm$ is small, the integrals of C_{++} and C_{--} need to be negative. This case implies an intermittent behavior of the dislocation positions: a group of dense dislocations is followed by a group of rare dislocations. Krivoglaz *et al.* (1983) imposed another condition, $C_{++}(\boldsymbol{\xi}) = C_{--}(\boldsymbol{\xi}) = -C_\pm(\boldsymbol{\xi})$, with the aim of simplifying the problem to a single correlation function. However, the correlations between dislocations with the same and with the opposite Burgers vectors are qualitatively different. Modeling of the relaxation in a system of initially uncorrelated dislocations (Zaiser *et al.*, 2001; Csikor & Groma, 2004) shows that the dislocations with opposite Burgers vectors reduce the elastic strain energy by making pairs, while dislocations with the same Burgers vectors tend to arrange in walls. In the present paper, we consider the simplest model that neglects the correlations between dislocations with the same Burgers vector direction, $C_{++}(\boldsymbol{\xi}) = C_{--}(\boldsymbol{\xi}) = 0$, and consider only correlations between the dislocations with opposite Burgers vectors, $C_\pm(\boldsymbol{\xi}) \neq 0$. We take equal densities of the dislocations with opposite Burgers vectors, $\rho_+ = \rho_- = \rho/2$. Then, the screening of the dislocation strain fields by surrounding dislocations is achieved when

$$\rho_+ \int C_\pm(\boldsymbol{\xi})\, \mathrm{d}\boldsymbol{\xi} = 1. \quad (26)$$

The normalization condition (26) allows $\rho_+ C_\pm(\boldsymbol{\xi})$ to be treated as a probability density. It describes dislocations of opposite sign generated in pairs, with the distance $\boldsymbol{\xi}$ between dislocations in the pair realized by the probability density $\rho_+ C_\pm(\boldsymbol{\xi})$. Correlations between pairs are absent. The total probability density of finding two dislocations of opposite sign at a distance $\boldsymbol{\xi}$ is equal to $\rho_+[C_\pm(\boldsymbol{\xi}) + 1]$: it is the sum of the probability density for the dislocations of the same pair, equal to $\rho_+ C(\boldsymbol{\xi})$, and dislocations of different pairs, equal to ρ_+, since the dislocations of different pairs are uncorrelated. Thus, the pair correlation function $C_\pm(\boldsymbol{\xi})$ for any dislocation distribution that provides the size-independent $T(\mathbf{r})$ given by (25) can be modeled by dislocation pairs with the distances in the pairs distributed with the probability density $\rho_+ C_\pm(\boldsymbol{\xi})$.

If the characteristic distance between dislocations in the pair R_c is small compared with the distance between pairs r_d, the pairs can be considered as well separated dislocation dipoles. The X-ray scattering from dislocation dipoles can be considered separately (Pototskaya & Ryboshapka, 1968; Krivoglaz, 1996) and we concentrate in the present analysis on the overlapping dislocation pairs, $R_\mathrm{c} \geq r_\mathrm{d}$.

The factor ς that is contained in the logarithmic term of (25) depends on the dislocation correlations. It was calculated by Krivoglaz *et al.* (1983) for several correlation functions of dislocation positions that they considered. We do not attempt to calculate the factor ς for the dislocation correlation models that we study, for the following reasons. First, the correlation function $C_\pm(\boldsymbol{\xi})$ and even its correlation length R_c are not known in any X-ray diffraction experiment. Even if the product ςR_c is determined by fitting the diffraction peaks with the use of (25), it is not possible to separate the two factors from the product. Secondly, rigorously speaking, the applicability of (25) requires the ratio $M = R_\mathrm{c}/r_\mathrm{d}$ of the correlation length R_c to the mean distance between dislocations r_d to be so large that $\ln M \gg 1$. However, as we already discussed in the *Introduction*, the fits of the experimental diffraction peaks from various systems to the peak profiles calculated on the basis of (25) give values of M in the range from 1 to 3. The broad applicability of (25) can be explained, as discussed above, by incorporating the corrections to (25) into the logarithmic term. Then, the factor ς depends on the correlation length R_c as well as the reflection order gb. It is therefore reasonable to consider the product $R = \varsigma R_\mathrm{c}$ as a single factor, the cutoff radius, that has to be determined from the fit of (25) to a measured, or Monte Carlo calculated, peak profile.

In §3 we calculate the X-ray diffraction peaks by generating dislocation pairs with various correlations and calculating the correlation function $G(\mathbf{r})$ directly from its definition (4), using the Monte Carlo method. The diffraction peak obtained by its Fourier transformation (3) has an advantage in comparison with the experiment in allowing direct access to the dislocation distribution. Then, by comparing the modeled diffraction peaks with the ones calculated using approximation (25), we can establish its practical applicability range.

2.3. Elastic strain energy of the dislocated crystal

The elastic strain energy of a crystal with dislocations is a result of the spatial integration of squared distortions, very similarly to (17). If dislocations are spatially uncorrelated (and not arranged in pairs), the elastic energy diverges as $\ln(L/a_0)$, where L is the sample size and a_0 is the dislocation core size, again very similarly to (20). Wilkens (1969, 1970*a*,*b*) proposed, based on this profound analogy, that the dislocations are correlated in such a way that their strains are screened by neighboring dislocations and hence L is not the sample size but a cutoff length of the screening. Hence, the cutoff length obtained from the fits of the diffraction peaks can be used to evaluate the elastic energy stored in the crystal with dislocations (Borbély *et al.*, 2000; Garabagh *et al.*, 2008).

The cutoff length R_el to describe the elastic energy is of the same order, but not necessarily the same as the cutoff length $R = \varsigma R_\mathrm{c}$ that describes the diffraction peaks in (25). The

uncertainty originates in the lower limit of the integral (18), which is of the order of gbr. In contrast, the lower integration limit of the elastic energy is the dislocation core size a_0. Below, in §3, we calculate the diffraction peak profiles and determine the cutoff lengths R that follow from them. Here we calculate, for the same screening models, the elastic cutoff lengths R_{el}. This can be done analytically for the pair correlation functions used in the Monte Carlo study below. Then, in §3.2, we compare the cutoff lengths for the diffraction peaks and the elastic energy, to obtain corrections needed for a reliable strain energy calculation from the X-ray data.

The condition (26) allows us to model the screening by uncorrelated pairs of dislocations, with the probability density of the distance s between dislocations in the pair equal to $\rho_+ C_\pm(s)$. We consider here all orientations of the pairs with equal probability, as simulated in the Monte Carlo study of screw dislocations in §3.2.

Since the pairs are not correlated, the mean of the squared total strain is equal to the sum of means of the squared strains of individual pairs. Hence, the elastic energy of the crystal with uncorrelated dislocation pairs is equal to the sum of elastic energies of the pairs. The elastic energy of a pair of screw dislocations per unit length of the dislocation lines is equal to $\mu b^2/(2\pi)\,\ln(s/a_0)$, where μ is the shear modulus and s is the distance between dislocations in the pair. Therefore, the elastic energy density of the crystal with dislocation pairs is

$$E = (\mu b^2/4\pi)\rho\langle\ln(s/a_0)\rangle, \tag{27}$$

since the density of the pairs is $\rho/2$.

The average (27) over the distance s between dislocations in the pair is

$$E = \left(\mu b^2/4\pi\right)\rho\int_0^\infty \ln(s/a_0)C_\pm(s)\,\mathrm{d}s. \tag{28}$$

For the exponential and Gaussian pair distribution functions $C_\pm(s)$ that are used in §3.2, the integration can be performed analytically using the integrals

$$\int_0^\infty \exp(-cx)\ln x\,\mathrm{d}x = -(\gamma + \ln c)/c \tag{29}$$

and

$$\int_0^\infty \exp\left[-(cx)^2\right]\ln x\,\mathrm{d}x = -\pi^{1/2}(\gamma + \ln 4 + 2\ln c)/(4c), \tag{30}$$

where $\gamma = 0.5772\ldots$ is the Euler constant.

The result of the integration (28) can be written as

$$E = \left(\mu b^2/4\pi\right)\rho\ln(R_{el}/a_0). \tag{31}$$

The ratio of the cutoff distance R_{el} in the elastic energy density (31) to the mean distance between dislocations in the pair R_c depends on the type of dislocation distribution. We find $R_{el}/R_c = \exp(-\gamma) \simeq 0.56$ for the exponential distribution and $R_{el}/R_c = 2^{1/2}\exp[-(\gamma + \ln 4)/2] \simeq 0.53$ for the Gaussian distribution. If all pairs have the same distance between dislocations (the unimodal distribution), the ratio is simply $R_{el}/R_c = 1$.

3. Monte Carlo calculation of the X-ray diffraction peaks

3.1. Intensity calculation by the Monte Carlo method

Both averaging over dislocation statistics (4) and the spatial integration (3) can be performed by the Monte Carlo method. Recently we have studied, in this way, the X-ray diffraction peaks from misfit dislocations in epitaxial films (Kaganer & Sabelfeld, 2009), where the spatial integration was three-dimensional. In the present work we need just a one-dimensional spatial integral (11). We find it computationally more efficient to use the Monte Carlo method for calculation of $G(x)$ and to apply the standard quadrature formulas to calculate the Fourier integral (11).

The correlation function could also be directly calculated from (7) and (9). Such a calculation is effective only when all dislocation pairs have the same distance between dislocations in the pair and the same orientation of each pair. In this case the dislocation pairs can be treated as one dislocation type in (5). The displacement $\mathbf{u}_\alpha(\mathbf{r})$ in that equation becomes the displacement field of the dislocation pair. Dislocation pairs of random widths and orientations, which we consider below, need to be treated as different defect types, which results in additional integrations in (7) and (9). In this case the Monte Carlo calculation of $G(x)$ is favored.

To calculate $G(x)$, a set of dislocations is generated first. The size of the simulation cell was always chosen large enough to avoid its influence on the result. The number of dislocations in a set varied in our calculations from hundreds to tens of thousands, depending on the correlation radius R_c. The dislocation distribution is defined by the screening condition (26): dislocations of opposite sign are generated by pairs, with the random distance $\boldsymbol{\xi}$ between dislocations in the pair sampled from the probability density $\rho_+ C_\pm(\boldsymbol{\xi})$. Then, the contribution of the nth generated dislocation set to the X-ray scattering intensity,

$$g_n(x) = \exp\{i[\mathbf{Q}\cdot\mathbf{U}(\mathbf{r}_1) - \mathbf{Q}\cdot\mathbf{U}(\mathbf{r}_2)]\}, \tag{32}$$

is calculated on a predefined grid of points x. The total displacements $\mathbf{U}(\mathbf{r})$ are calculated, as a sum (5) over dislocation displacements, at two points $\mathbf{r}_1$ and $\mathbf{r}_2$ separated by x. The function $G(x)$ is approximated by

$$G_N(x) = (1/N)\sum_{n=1}^{N} g_n(x), \tag{33}$$

where N is the number of the generated dislocation sets. The statistical error of the approximation can be obtained by calculating in parallel the dispersion of $g_n(x)$, as we have done in the previous study of the misfit dislocations (Kaganer & Sabelfeld, 2009).

The numerical Fourier transformation of the correlation function is fairly sensitive to the edge of the x range where the correlation function $G(x)$ is calculated. To avoid unphysical oscillations in the calculated $S(q)$ and reduce the amount of computations, we include the finite experimental resolution in the calculations from the very beginning, as has been done in the study of the X-ray scattering from misfit dislocations

(Kaganer *et al.*, 1997; Kaganer & Sabelfeld, 2009). The convolution of the intensity (11) with a resolution function $\mathcal{R}(q)$ can be rewritten, using the convolution theorem, as the Fourier transformation of the product

$$S(q) = \int_{-\infty}^{\infty} G(x)\tilde{\mathcal{R}}(x)\exp(iqx)\,\mathrm{d}x, \qquad (34)$$

where $\tilde{\mathcal{R}}(x)$ is the Fourier transformation of $\mathcal{R}(q)$. This is quite similar to the appropriate choice of the resolution in the X-ray diffraction experiment. An example is given in Fig. 2 of Kaganer & Sabelfeld (2009). In the Monte Carlo calculations presented below, we always choose a Gaussian function $\tilde{\mathcal{R}}(x)$ so broad [and therefore the resolution function $\mathcal{R}(q)$ so narrow] that the 'instrumental' broadening of the peak is negligible. Accordingly, we do not include the resolution in the approximate calculations below.

3.2. Diffraction peaks from correlated screw dislocations

First, let us consider screw dislocations, which served as a touchstone in the initial studies (Krivoglaz & Ryboshapka, 1963; Wilkens, 1970*a*,*b*). Burgers vectors and displacements of screw dislocations have only a z component, along the dislocation lines. Only the z component of the scattering vector $\mathbf{Q}$ is essential, and, for a dislocation at the origin, $\mathbf{Q}\cdot\mathbf{u} = gb\arctan(y/x)$, where $gb = Q_z b_z/2\pi$. Figs. 1(*a*) and 1(*b*) illustrate the generated dislocation sets. They present a small part of the simulation area: the linear sizes of the whole simulated distribution vary from tens to hundreds, in units of the average dislocation distance. Dislocations with the opposite Burgers vectors (shown by open and filled circles) are generated by pairs. Orientations of the vectors connecting two dislocations of the pair are chosen at random from 0 to 2π, and the distances between dislocations in the pairs are chosen from the exponential distribution with the mean distance R_c. Below we also study other distributions of the dislocation pair widths. The choice of the exponential distribution agrees with the results of Csikor & Groma (2004). They generated a two-dimensional array of initially uncorrelated edge dislocations and allowed them to move and hence reduce the elastic energy. The final state reveals an exponential distribution of the pairs of opposite sign dislocations, with $R_c \simeq 0.5$ [see equation (32) by Csikor & Groma (2004)].

Dislocation distributions simulated for two different correlation lengths, $R_c = 1$ and 5, are shown in Figs. 1(*a*) and 1(*b*), respectively. Hereafter, we take the mean distance between dislocations $r_d = \rho^{-1/2}$ as the unit length. Accordingly, the wavevectors q are measured in units of r_d^{-1}.

The correlation functions $G(x)$ calculated by (33) using the Monte Carlo method are presented in Fig. 1(*c*). They are even, $G(-x) = G(x)$, due to the symmetry of the problem. Hence, the Fourier transformation (34) is reduced to

$$S(q) = 2\int_0^{\infty} G_s(x)\cos(qx)\,\mathrm{d}x, \qquad (35)$$

where $G_s(x)$ is the even correlation function for screw dislocations, and we skip the resolution function in the formulas. Diffraction peaks obtained by Fourier transformation (35) of these correlation functions are shown in Fig. 2 by thick gray lines. Since the diffraction peaks are calculated without any simplifying approximation, they are well suited, better than the experimental data, to test the approximate description of the peak profiles.

Our analysis is based on the approximation (20) and we denote $R = \varsigma R_c$. The length R can be considered as a 'cutoff length', the quantity that can be determined from an experiment without knowing the correlation length R_c. We also modify the expression (20), as was suggested earlier (Kaganer *et al.*, 2005), to avoid the unphysical oscillations that arise from the Fourier integration in finite limits, and to be able to extend the integration over x to infinite limits. We represent the correlation function as

$$G_s(x) = \exp\left[-\frac{1}{2}\chi_s(gb)^2\rho x^2\ln\frac{2R/gb + x}{x}\right]. \qquad (36)$$

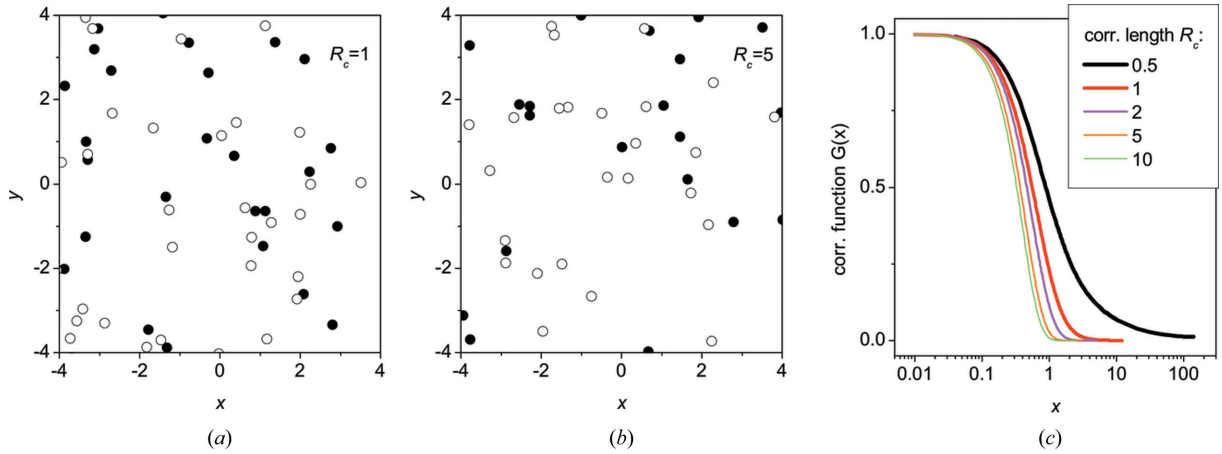

Figure 1
Monte Carlo calculation of the correlated screw dislocations. (*a*, *b*) Dislocation arrangements for the exponential pair distribution function with correlation lengths $R_c = 1$ and 5. Open and filled circles represent dislocations with the opposite Burgers vectors. (*c*) Correlation functions $G(x)$ calculated by the Monte Carlo method.

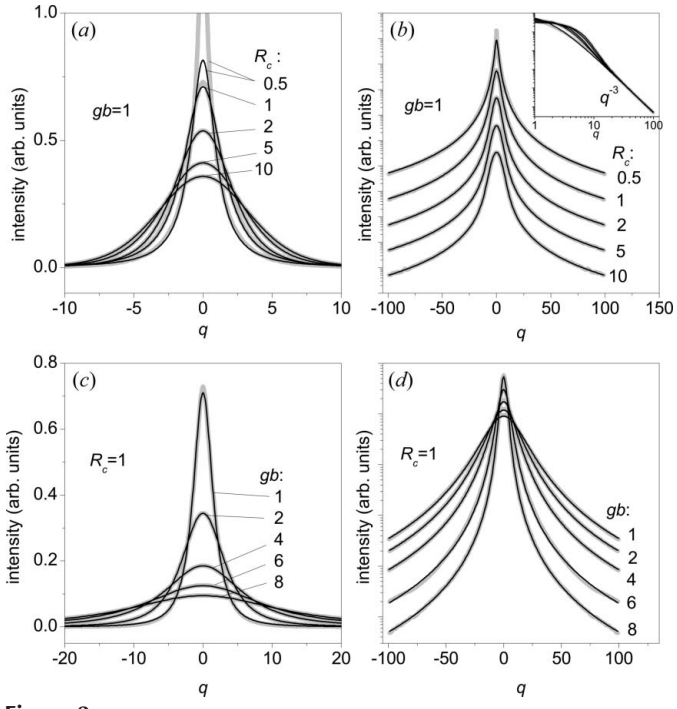

Figure 2
X-ray diffraction peaks for correlated screw dislocations. Results of the Monte Carlo calculation (thick gray lines) are fitted to equations (35) and (36) (thin black lines). (*a*, *b*) Calculations for different correlation lengths at the same reflection with $gb = 1$. (*c*, *d*) Calculations in different reflections for the same correlation length $R_c = 1$. The fits in (*a*, *c*) are made on a linear scale, by minimizing the mean-squared difference of intensities. The fits in (*b*, *d*) are made on a logarithmic scale, by minimizing the mean-squared difference of the logarithms of intensities. Curves in (*b*, *d*) are offset vertically for clarity.

The choice of the functional form (36) is discussed in Appendix *A*. The factor 2 in the logarithmic term is introduced to keep agreement with the Wilkens definition of the parameter $M = R\rho^{1/2}$.

The angular factor χ_s for screw dislocations, with **b** along the *z* axis and **r**, $\boldsymbol{\xi}$ in the *xy* plane, can be easily calculated. It is obtained by integrating in (19) the factor $\Psi = \cos\phi$, where ϕ is the angle between **r** and $\boldsymbol{\xi}$. Hence, we have $\chi_s = \pi$. We fit the intensities calculated by the Monte Carlo method by an approximate peak profile given by (35) and (36). It contains just two free parameters, the dislocation density ρ and the cutoff length *R*.

Fig. 2 shows examples of the fits of the peak profiles calculated by the Monte Carlo method (thick gray lines) to the Fourier-transformed correlation function (36) (thin black lines). Excellent fits are obtained in the whole range of parameters, except the narrow central peak of the top curve in Figs. 2(*a*) and 2(*b*). In this case the mean distance between dislocations in the pair $R_c = 0.5$ is smaller than the mean distance between dislocations, so that non-overlapping dislocation dipoles are formed and, because of the rather small size of the simulated system, the coherent scattering peak becomes visible. We do not consider small correlation lengths $R_c < 1$ and the coherent peaks in the further analysis.

We fit the diffraction peaks to one and the same approximation (36) for the correlation function in two different ways: either the mean-squared difference between the Monte Carlo calculated intensity and the approximation is minimized (the linear fit) or the mean-squared difference of their logarithms is minimized (the logarithmic fit). These two ways of fitting correspond to different experiments. In the X-ray diffraction study of dislocations in single crystals, in particular in epitaxial films (Kaganer *et al.*, 2005, 2009), the scattered intensity can be measured in a fairly large momentum range around each Bragg peak. Then, the asymptotic scattering at large *q* can be measured. The insert in Fig. 2(*b*) shows that all diffraction peaks converge to the same q^{-3} asymptote. This asymptotic behavior is a general feature of the dislocation strain field. It is properly described by the correlation function (36) due to the logarithmic term in the exponent. This asymptotic behavior is observed experimentally (Groma, 1998; Groma & Székely, 2000; Kaganer *et al.*, 2005, 2006) and allows accurate dislocation density determination. The logarithmic fits are shown in Figs. 2(*b*) and 2(*d*). The fitted parameters, the dislocation density ρ and the cutoff distance *R*, are primarily determined by the asymptotic scattering region. Such fits were used by Kaganer *et al.* (2005) in the study of threading dislocations in GaN epitaxial films. On the other hand, these fits are not perfect at the maxima of scattered intensity.

In the studies of polycrystalline or powder samples, the scattered intensity can be attributed to a certain diffraction peak only in a limited *q* range. The asymptotic regions of different peaks overlap after the powder average over random orientations of the crystallites. It remains to use the central parts of the peaks and fit them on the linear scale. The linear fits in Figs. 2(*a*) and 2(*c*) primarily describe the intensity distribution near the maxima. Note that the *q* range in these figures is much smaller than in Figs. 2(*b*) and 2(*d*). The peaks are also well described by the correlation function (36), except the case of small correlation lengths $R_c < 1$, which we do not analyze in this paper.

The fit results for both linear and logarithmic fits are summarized in Fig. 3. The fit parameters for the linear fits are shown by open symbols, and those for logarithmic fits by full symbols. We compare four different types of dislocation correlations. The distance between dislocations in the pair follows either exponential distribution (squares on the figures), Gaussian distribution (circles) or all dislocation pairs have the same separation R_c (up triangles). We also simulated the Wilkens restrictedly random dislocation distribution (down triangles). This model is described in more detail below, and additional results are presented in Fig. 4.

Since the mean distance between dislocations is taken as the unit length in Monte Carlo calculations, the dislocation density is just 1 in these units. The dislocation densities obtained by the fits to (36) are very close to this value. For logarithmic fits, when $R_c \geq 2$, the values obtained for different dislocation distributions are within 1 ± 0.04. Even for $R_c = 0.5$, which is out of the expected applicability range of the approximation (36), the error is less than 40%. Such accuracy is reached due to the leading contribution from the asymptotic scattering region. This accuracy is even better than needed for the analysis of the experimental data, where larger errors can be

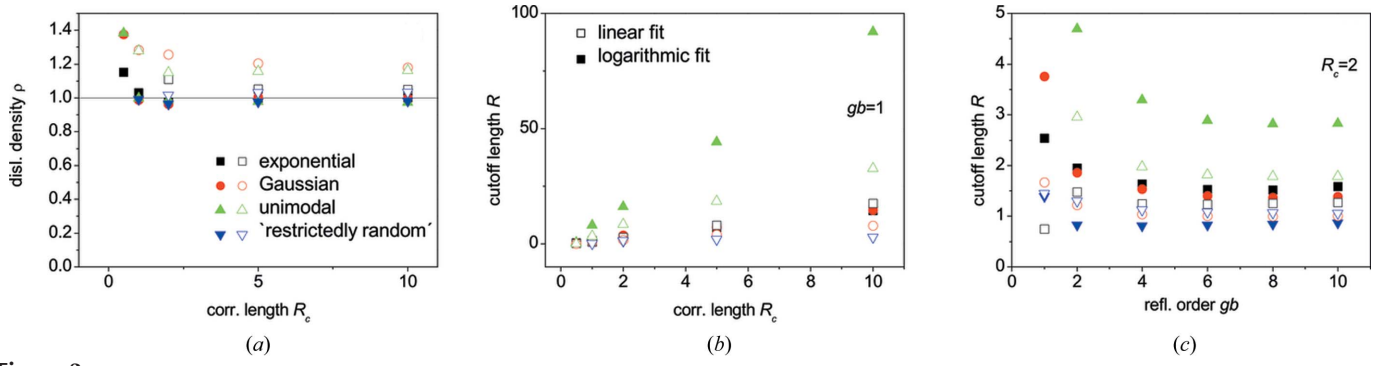

Figure 3
Parameters obtained by the fits of the calculated peaks for different dislocation distributions: (*a*) dislocation density ρ at different correlation lengths R_c, (*b*, *c*) cutoff length R at different correlation lengths R_c and reflection orders gb. The results of the linear fits are shown by open symbols and those of logarithmic fits by full symbols.

expected from non-uniformity of the dislocation distribution and bending of the dislocation lines. These results provide a firm ground for accurate dislocation density determination from the X-ray diffraction peaks with the use of the approximation (36) (Kaganer *et al.*, 2005). The linear fit overestimates the dislocation density up to 30%, depending on the type of dislocation correlations. Such accuracy seems sufficient for practical applications, however. Thus, the fit results show that the approximation (36) provides an accurate and reliable way for dislocation density determination from the X-ray diffraction peak profiles.

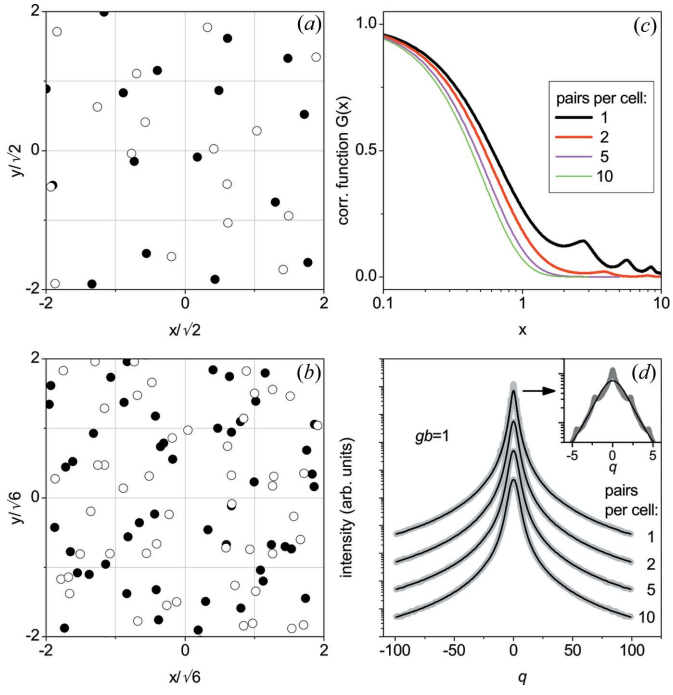

Figure 4
Monte Carlo calculation of the diffraction peaks in the Wilkens restrictedly random dislocation distribution model. (*a*, *b*) Dislocation arrangements with 1 or 3 dislocation pairs per cell. Open and filled circles represent dislocations with the opposite Burgers vectors. (*c*) Correlation functions $G(x)$ calculated by the Monte Carlo method. (*d*) Diffraction peaks calculated by the Monte Carlo method (thick gray lines) and the fits to the formulas (35) and (36) (thin black lines). The curves are shifted vertically for clarity. The insert in (*d*) magnifies the peak of the top curve (one pair of dislocations per cell).

The second parameter obtained from the fits, the cutoff distance R, is shown in Figs. 3(*b*) and 3(*c*). It coincides with the Wilkens dimensionless parameter M, since the mean distance between dislocations is taken as a unit length. A strong variation of this parameter, depending on the type of the dislocation correlations, is evident. R is approximately proportional to the input parameter, the correlation length R_c, so that the ratio $\varsigma = R/R_c$ is close to a constant. For the logarithmic fit, the value of ς for the first-order reflection, $gb = 1$, is approximately 0.3 for the Wilkens restrictedly random dislocation distribution, 1.5 for the exponential and Gaussian distributions, and 9 when all dislocation pairs have the same separation (unimodal distribution). For the linear fit, it is 0.3 for the Wilkens restrictedly random dislocation distribution, 0.8 for the Gaussian distribution, 1.7 for the exponential distribution and 3 for the unimodal distribution. The cutoff distances R also depend on the reflection order, see Fig. 3(*c*), but they approach constant values for $gb \geq 5$. Note that at large gb the cutoff length R is close to the correlation length R_c chosen on input.

We now describe the calculations for the Wilkens restrictedly random dislocation distribution model (Wilkens, 1970*a*,*b*, 1976) in more detail. In this model, the crystal is subdivided into cells of equal size, each cell containing the same number of dislocations, half of them having a Burgers vector $+\mathbf{b}$ and another half $-\mathbf{b}$. Fig. 4(*a*) shows such a dislocation distribution with one pair of dislocations per cell. The cell area is equal to 2, since it contains two dislocations. Similarly, Fig. 4(*b*) shows a distribution with three dislocation pairs per cell; the cell area is 6. The dislocations are distributed in the cells according to the Wilkens model, but the dislocation displacement field is not restricted to the cell that contains the dislocation. Rather, it contributes to the total displacements in the whole simulated area.

The results of the Monte Carlo calculation of the correlation function $G(x)$ for different cell sizes are presented in Fig. 4(*c*). They are similar to those in Fig. 2, except for the case of one dislocation pair per cell, where the oscillations due to the cellular structure are evident. Diffraction peaks calculated

by Fourier transformation (35) are shown in Fig. 4(*d*) by thick gray lines. The cellular structure for one dislocation pair per cell is visible also in the diffraction peak [see insert in Fig. 4(*d*)]. The fits by formula (36) describe the peaks well (thin black lines).

We can compare now the cutoff distances for elastic energy R_{el} from §2.3 with the cutoff distances R obtained in the present section by fits of the diffraction curves. The values of R depend on the diffraction order, see Fig. 3(*c*), but approach constant values for large gb (practically, $gb \geq 5$). Using these values for large gb, we find that, for all three types of distance distributions, the ratio R/R_{el} is 1.2 for the linear fits of diffraction peaks and 1 for the logarithmic fits, with a scattering of ± 0.1 for different distributions. Since three different types of distance distributions give very close ratios, we expect that these values can be used to obtain the elastic cutoff length R_{el} and the elastic energy density (31) for any dislocation correlations. For low reflection orders, Fig. 3(*c*) reveals a strong dependence of the diffraction cutoff length R on the reflection order. For example, for the first-order reflection, $gb = 1$, and the linear fit of the diffraction peaks, the ratio R/R_{el}, varies from 2.2 for the exponential distribution to 8 for the unimodal distribution. The result strongly depends on the distribution of the dislocation distances in the pairs. The distribution is not known in advance and cannot be determined from the diffraction peaks. Hence, the use of low-order reflections introduces a large uncertainty in the elastic cutoff length and in the estimate of the strain energy. The cutoff lengths obtained from the higher-order reflections, $gb \geq 5$, do not depend on the distribution function and provide more reliable determination of the elastic energy stored in the dislocated crystal.

3.3. Edge dislocations and peak asymmetry

For the screw dislocations considered above, the Burgers vectors are along the dislocation lines. The vector **l** in the plane perpendicular to the dislocation lines directed from the dislocation with Burgers vector $-\mathbf{b}$ to that with $+\mathbf{b}$ is always perpendicular to **b**. We took all orientations of **l** for pairs of screw dislocations as equally probable in the calculations of the previous section. For edge dislocations studied in this section, both **b** and **l** lie in the plane perpendicular to the dislocation lines. If **b** is perpendicular to **l**, the dislocation pair can correspond to either a stripe of an extra atomic plane inserted between the dislocation lines or a stripe of an atomic plane removed between the lines.

When one type of dislocation pair prevails, such dislocation distributions can be treated as polarized (Groma *et al.*, 1988; Ungár *et al.*, 1989; Groma & Monnet, 2002), since there is a preferred direction from a dislocation with the Burgers vector $-\mathbf{b}$ to that with the Burgers vector $+\mathbf{b}$ which can be considered as polarization. However, the dislocation pairs do not form physical dipoles, like electrical charges. Rather, a symmetry plane perpendicular to the line connecting dislocations in the pair is preserved. We call such dislocation pairs interstitial if a stripe of an atomic plane is inserted between the dislocation lines, and vacancy type if a stripe is removed. If both interstitial and vacancy dislocation pairs are present with equal probabilities, the diffraction peaks are very similar to those from screw dislocations, and we do not present them here. New effects arise when the probabilities are not equal.

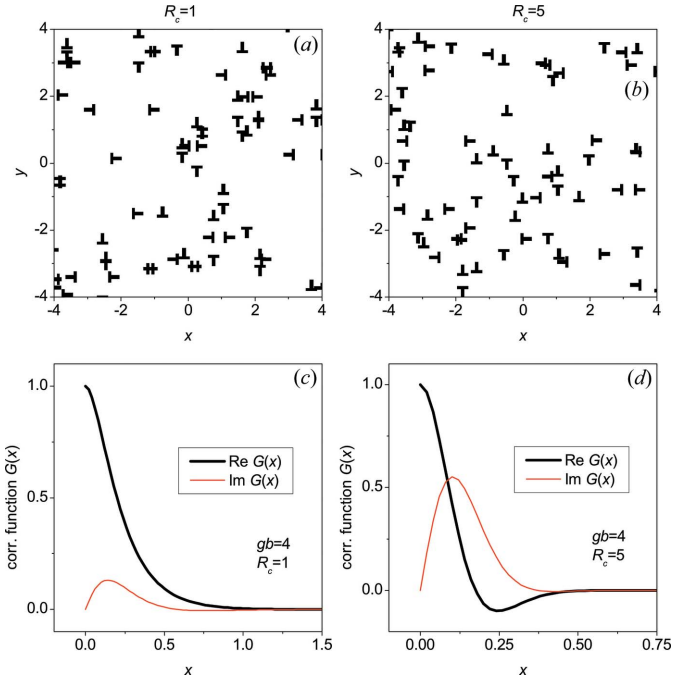

Figure 5
Monte Carlo calculation of the correlated edge dislocations. (*a*, *b*) Dislocation arrangements of vacancy-type dislocation pairs for the exponential pair distribution function with the correlation lengths $R_c = 1$ and 5. The pairs are oriented in two orthogonal directions. (*c*, *d*) Correlation functions $G(x)$ calculated by the Monte Carlo method.

Figs. 5(*a*) and 5(*b*) show distributions of only vacancy pairs. The pairs are oriented in two orthogonal directions, to keep the fourfold symmetry. The positions of the pair centers are random and uncorrelated. The distances between dislocations in the pairs are taken from the exponential distribution with the mean distance R_c equal to 1 and 5 in Figs. 5(*a*) and 5(*b*), respectively.

The prevalence of either interstitial- or vacancy-type dislocation pairs and the corresponding asymmetry of the diffraction peaks described below is not specific to edge dislocations. It could also arise for screw dislocations, if a preferred direction from $-\mathbf{b}$ to $+\mathbf{b}$ is realized. However, an asymmetry in the distribution of the edge dislocation pairs seems more plausible. The vacancy-type pairs in Figs. 5(*a*) and 5(*b*) can be a result of condensation of vacancies in the crystal. Similarly, a condensation of interstitials would result in the opposite case of interstitial dislocation pairs.

Figs. 5(*c*) and 5(*d*) present the correlation function (4) calculated for these dislocation distributions by the Monte Carlo method. The correlation function is no longer a real value but contains also an imaginary part. As a result, Fourier transformation (34) of the correlation function gives rise to the diffraction peaks shown in Fig. 6. The peaks are asym-

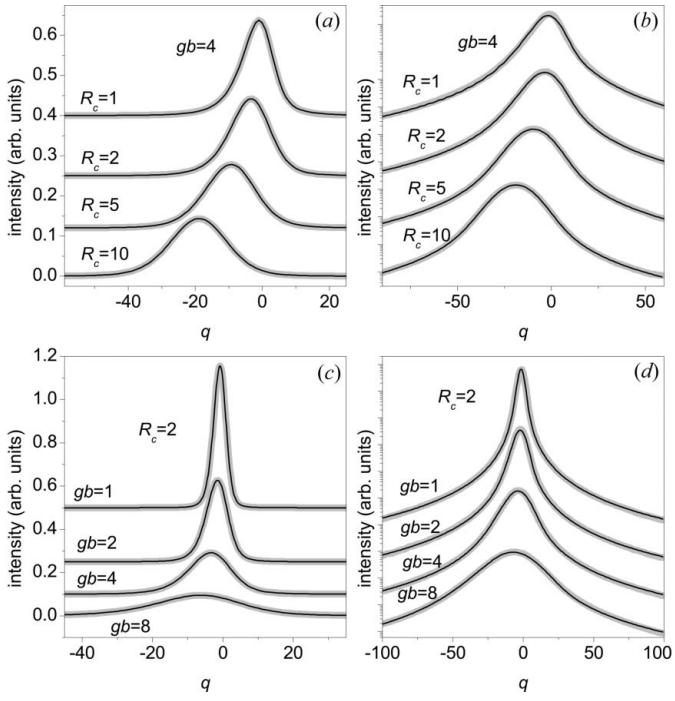

Figure 6
X-ray diffraction peaks for correlated edge dislocations. Results of the Monte Carlo calculation (thick gray lines) are fitted to equations (38) and (41) (thin black lines). (*a*, *b*) Calculations for different correlation lengths at the same reflection with $gb = 4$. (*c*, *d*) Calculations in different reflections for the same correlation length $R_c = 2$. The fits in (*a*, *c*) are made on a linear scale, by minimizing the mean-squared difference of intensities. The fits in (*b*, *d*) are made on a logarithmic scale, by minimizing the mean-squared difference of the logarithms of intensities. Curves are offset vertically for clarity.

metric and their maxima are shifted with respect to $q = 0$. These asymmetric peaks are obtained for a homogeneous dislocation distribution, in contrast to the asymmetric peaks due to an inhomogeneous dislocation distribution (Groma *et al.*, 1988; Groma, 1998; Groma & Monnet, 2002). The asymmetry increases with the increasing reflection order gb and decreases with the increased correlation length R_c.

Equations (35) and (36) are not sufficient in the present case and need to be extended. We can return to the general equations of §2 and apply them to uncorrelated dislocation pairs. Each term in the sum (5) is now the displacement field of the pair and the function $T(\mathbf{r})$ in (6) is given by (7). Further terms of the cumulant expansion are absent, since the pairs are not correlated. The difference of displacements can be expanded in Taylor series (13) under the same assumptions as given in §2.2. Then, the exponent in (8) is expanded in a power series. We denote the term of the order of r^n as $T^{(n)}(\mathbf{r})$, to distinguish it from the terms of the cumulant expansion in (9).

The first-order term $T^{(1)}(\mathbf{r})$ is non-zero if either vacancy- or interstitial-type dislocation pairs predominate. This term (15) is imaginary and linear over $\mathbf{r}$, so that it can be written as $T^{(1)}(\mathbf{r}) = iq_0x$. Calculating the average strain for uncorrelated dislocation pairs with the mean distance between dislocations in the pair R_c, we obtain

$$q_0 = gb\rho R_c/2. \tag{37}$$

Here $gb = Q_x b_x/2\pi$, and the factor $1/2$ takes into account that the peak shift is due to the pairs extended along the y axis, while those along the x axis do not contribute to the peak shift. Introduction of the first-order term $T^{(1)}(\mathbf{r})$ into (34) transforms the exponential term to $\exp[i(q + q_0)x]$, *i.e.* the average strain provides a shift of the Bragg peak, as it should do.

The second-order term $T^{(2)}(\mathbf{r})$ is real. With the same reasoning as above, based on the discussion in Appendix *A*, we represent it in the same way as equation (36),

$$G_e(x) = \exp\left[-\frac{1}{2}\chi_e(gb)^2\rho x^2 \ln\frac{2R/gb + x}{x}\right], \tag{38}$$

where the contrast factor χ_e has to be calculated now for edge dislocations. The calculation for edge dislocations with the Burgers vector in x and y directions gives, respectively,

$$\chi_{ex} = \pi\frac{5 - 4\nu(3 - 2\nu)}{8(1 - \nu)^2}, \quad \chi_{ey} = \pi\frac{1 - 4\nu + 8\nu^2}{8(1 - \nu)^2}, \tag{39}$$

where ν is the Poisson ratio. We consider equal densities of dislocations along and perpendicular to $\mathbf{Q}$, so that the contrast factor is the average $\chi_e = (\chi_{ex} + \chi_{ey})/2$. For the Poisson ratio $\nu = 1/3$, it is equal to $\chi_e = 11\pi/32$.

Evaluation of the peak asymmetry requires the third-order term $T^{(3)}(\mathbf{r})$, *cf.* Groma *et al.* (1988). It is imaginary and the calculation similar to that of the second-order term in §2.2 shows that this term is proportional to $i\rho(gb)^3r^3\ln(\varsigma'''R_c/gbr)$, where $\varsigma''' \simeq 1$ is a constant. We define the function

$$\varphi(x) = a\rho(gb)^3x^3\ln(R_a/gbx), \tag{40}$$

which contains two parameters, the asymmetry a and the asymmetry cutoff length $R_a = \varsigma'''R_c$. Then, (34) can be represented as

$$S(q) = 2\int_0^\infty G_e(x)\cos\big[(q + q_0)x + \varphi(x)\big]\,dx. \tag{41}$$

Thin black lines in Fig. 6 are fits of the peak profiles calculated by the Monte Carlo method to (38) and (41). The fit parameters are the peak position q_0, the dislocation density ρ, the cutoff length R, the asymmetry a and its cutoff length R_a. The peaks are perfectly described by (38) and (41). The peak position is given by (37). The results of the fits of the dislocation density ρ and the cutoff length R are very similar to the results for screw dislocations in Fig. 3, and we do not present them. The asymmetry a and its cutoff length R_a are shown in Fig. 7. We find $a \simeq 0.1$. The asymmetry cutoff length $R_a \geq 1$ shows rather large scattering of the values.

4. Discussion and summary

The kinematical X-ray diffraction theory allows, in principle, calculation of the scattered intensity for a crystal with any distribution of defects and their displacement fields. Practical calculation, however, requires averaging (4) over statistics of the defect distribution and spatial integration (3). Both integrations can be performed simultaneously by the Monte Carlo method (Kaganer & Sabelfeld, 2009). The powder average over crystal orientations, as well as the intensity integration

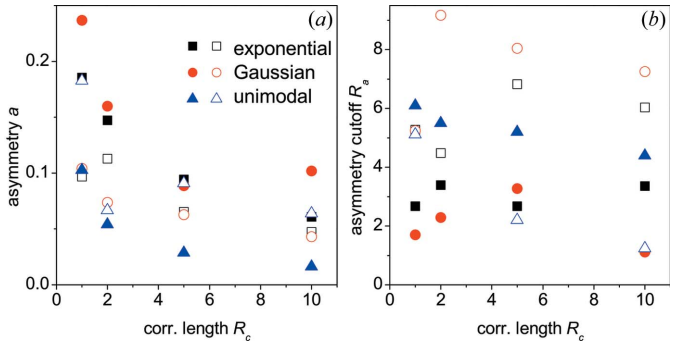

Figure 7
Asymmetry parameters obtained by the fits of the calculated peaks for different dislocation distributions: (*a*) asymmetry *a* and (*b*) asymmetry cutoff length R_a for different correlation lengths R_c. The results of the linear fits are shown by open symbols and those of the logarithmic fits by full symbols.

over a wide-open detector in double-crystal diffraction from a single crystal, reduces the spatial integration to a one-dimensional integral (11). In this case the spatial integration can be performed by standard quadratures, while the statistical average (4) is performed by the Monte Carlo integration. This is done in the present work.

Monte Carlo calculations include essential features of the experiment. The dislocations are distributed at random over a volume large enough to exclude the finite size effects. In our practical calculations the number of dislocations in the simulated sample varies from hundreds to tens of thousands, depending on the correlation length of the dislocation distribution. The correlation function (4) is calculated for separations much smaller than the sample size but large enough to reveal the whole diffuse scattering pattern. The finite coherence length of a diffraction experiment is included in the intensity calculation (34). The coherence length is taken large enough to avoid broadening of the diffuse peak.

The Wilkens idea, that the dislocations arrange to avoid the divergence of the elastic energy, and the divergence of the diffraction peak width is avoided at the same time, permits a much broader class of dislocation correlations than just the original restrictedly random dislocation distribution. The arrangement of the dislocations with opposite Burgers vectors in pairs provides the screening of the long-range strain field and results in peak widths limited by the mean distance between dislocations in the pair. The mean distance in the pair can be larger than the average distance between dislocations, so that the pairs overlap and cannot be considered as dipoles with a dipole width small compared with the distance between dipoles. Moreover, any screening due to pair correlations between dislocations can be modeled by dislocation pairs with the appropriate distribution of distances between dislocations in the pair.

We have calculated diffraction peak profiles for different types of pair correlations. The widths of the dislocation pairs were distributed according to exponential and Gaussian laws, or all pairs had the same distances. We also simulated the Wilkens restrictedly random distribution by dividing the sample area into cells with an equal number of uncorrelated dislocations in each cell. In contrast to the original Wilkens model, the dislocation displacement field is not restricted to the cell containing the dislocation but penetrates into other cells. The peaks are qualitatively similar for all correlation types. They possess the same q^{-3} asymptote at large q.

The correlation function (36) is slightly modified with respect to the original form (1) to allow smooth calculation of the Fourier integral. We show in Appendix *A* that this modification is practically undistinguishable from the bulky formula derived by Wilkens for his restrictedly random dislocation distribution. The dislocation density obtained from the fit of the Fourier-transformed correlation function (36) to the Monte Carlo calculated peaks practically coincides with the density chosen as input to the Monte Carlo calculations. This justifies the use of equation (36) for the dislocation density determination from the experimental peaks. The second parameter of the fit, the cutoff length, is close to the correlation length of the dislocation pair distribution only in high-order reflections, $gb \geq 5$. This cutoff length can be safely used to estimate elastic energy stored in the dislocated crystal. For low reflection orders, the cutoff length depends on the type of correlations and on the reflection order. We considered the pairs of edge dislocations formed by removing a stripe of an atomic plane between dislocation lines (vacancy-type pairs). A homogeneous distribution of such pairs gives rise to asymmetric peaks. The asymmetry increases with the reflection order and decreases when the correlation length of the dislocation pairs is increased. The symmetric part of the intensity is described by the same correlation function (38). The asymmetry is described by the higher-order term and leads to equation (41) for the intensity calculation.

APPENDIX *A*
Approximate expressions for $G(x)$

The expression (25) for the correlation function $T(\mathbf{r})$ was derived under the assumption $r \ll R_c$. The calculation of the intensity distribution by the Fourier transformation (35) requires a formula that could be used in the whole range of r from zero to infinity. The formula (25) cannot be used in such a range without modification, since the logarithm becomes negative for $r > R_c$ and the integral diverges. Although $G(x)$ is exponentially small for $x \geq R_c$, it is not possible just to take $G(x) = 0$ for $x > R_c$: a rigid edge of the integration range gives rise to unphysical oscillations when making the Fourier transformation. Hence, one needs to replace (25) with a function that has the same behavior as (25) for small r but remains positive and behaves smoothly on the whole interval $(0, \infty)$. Wilkens (1970*b*) represented the correlation function (25) as

$$G_s(x) = \exp\left[-(1/2)\chi(gb)^2\rho x^2 f(\eta)\right]. \qquad (42)$$

For the first reflection order, $gb = 1$, the argument η is defined as $\eta = x/2R_p$. We consider the case $gb = 1$ first, and discuss the gb dependence afterwards. In the restrictedly random dislocation distribution model, R_p is the radius of cells containing equal numbers of positive and negative positionally uncorre-

lated dislocations. In this model, Wilkens (1970*b*) proposed a bulky formula for $f(\eta)$,

$$f(\eta) = -\ln\eta + \frac{7}{4} - \ln 2 + \frac{256}{45\pi\eta} + \frac{2}{\pi}\left(1 - \frac{1}{4\eta^2}\right)\int_0^{\eta}\frac{\arcsin y}{y}\,\mathrm{d}y - \frac{1}{\pi}\left(\frac{769}{180\eta} + \frac{41}{90}\eta + \frac{\eta^3}{45}\right)\left(1-\eta^2\right)^{1/2} - \frac{1}{\pi}\left(\frac{11}{12\eta^2} + \frac{7}{2} + \frac{\eta^2}{3}\right)\arcsin\eta + \frac{\eta^2}{6} \qquad (43)$$

for $\eta \leq 1$, and

$$f(\eta) = \frac{256}{45\pi\eta} - \left(\frac{11}{24} + \frac{1}{4}\ln 2\eta\right)\frac{1}{\eta^2} \qquad (44)$$

for $\eta \geq 1$. Although this formula has been cited many times in the literature, we are not aware of its derivation. This function is shown in Fig. 8(*a*) by the full line. The diffraction peak profile obtained from it is presented, also by full lines, in Figs. 8(*b*) and 8(*c*) on linear and logarithmic scales, respectively.

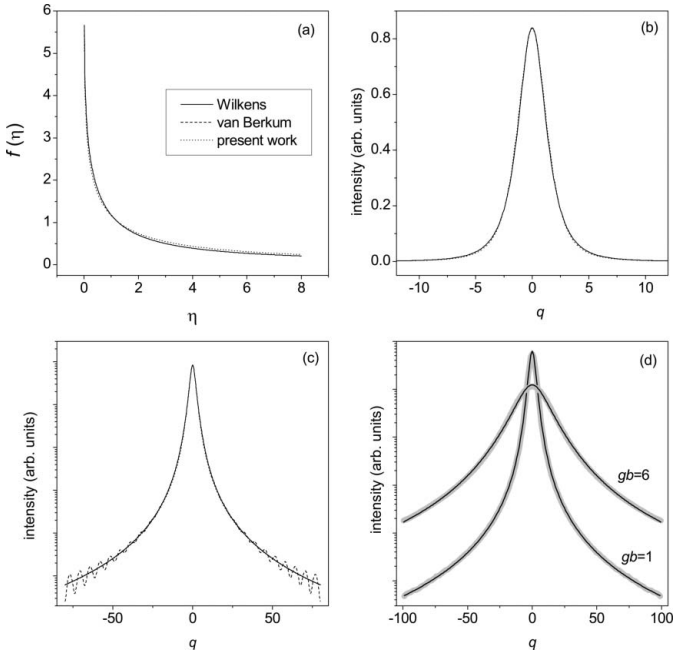

Figure 8
(*a*) The function $f(\eta)$ defined by Wilkens (1970*b*) (full line), its modification by van Berkum (1994) (dashed line) and the function (46) used in the present work (dotted line). (*b*, *c*) Diffraction peak profiles calculated with these three functions on linear and logarithmic scales, respectively. (*d*) Diffraction peaks calculated by the Monte Carlo method for the Wilkens restrictedly random dislocation distribution model with two dislocation pairs per cell (thick gray lines) and fits using equations (42)–(44) (thin black lines).

Let us consider now the higher-order reflections. The original formula by Wilkens (1970*b*) contained, instead of $f(\eta)$ in (42), a term $[f(\eta) - K]$, with the parameter K approximated as $K \simeq 1 + \ln gb$. Since $f(\eta)$ tends to zero for $\eta \to \infty$, the introduction of $K > 0$ into (42) would result in divergence of the Fourier integral. Later papers, *e.g.* Scardi & Leoni (2002), Kužel (2007), cite the Wilkens formula without including this term, in a way equivalent to (42). The gb dependence of K can be included in (43) by writing $\ln(gb\eta)$ instead of $\ln\eta$. This correction agrees with our equation (25) and the results of the Monte Carlo study (see Fig. 3). If this correction is not made, the parameter R_p in the definition $\eta = x/2R_\mathrm{p}$, considered as a free parameter in a fit of the diffraction peak (the cutoff radius), will be approximately proportional to gb. We define $\eta = gbx/2R_\mathrm{p}$ in equation (42), to obtain the same cutoff radius for all reflections.

In Fig. 8(*d*), thick gray lines are the result of Monte Carlo calculation of the diffraction peaks in the restrictedly random dislocation model. Each cell contains two pairs of dislocations with opposite Burgers vectors. Two reflections are compared, $gb = 1$ and 6. Two dislocation pairs per cell are simulated. Thin black lines are the fits to Fourier transformation (35) of the correlation function (42) with two fit parameters, the dislocation density ρ and the cutoff radius R_p. The dislocation density determined from the fits is $\rho = 0.90$ and 0.83 for the two reflections. The mean distance between dislocations is taken as the unit length, so that $\rho = 1$ is the input of the Monte Carlo simulations. The cutoff radius obtained from the fits is $R_\mathrm{p} = 0.55$ and 0.44 for the two reflections.

Scardi & Leoni (2002) proposed to use a simplification of the bulky formula (43), referring to van Berkum (1994),

$$f(\eta) = -\ln\eta + \frac{7}{4} - \ln 2 + \frac{\eta^2}{6} - \frac{32\eta^3}{225\pi} \qquad (45)$$

for $\eta \leq 1$. The same formula (44) remains to be used for $\eta \geq 1$. This function is shown in Fig. 8(*a*) by the dashed line: it is undistinguishable from (43) in the scale of the figure. It is also undistinguishable when the diffraction peak is plotted in the linear scale in Fig. 8(*b*). However, when the asymptotic scattering is revealed in Fig. 8(*c*), the distinction becomes clearly visible: formula (45) gives rise to unphysical oscillations of period $\triangle q = 2\pi$. The origin of these oscillations is evident. The derivative $\mathrm{d}f/\mathrm{d}\eta$ is discontinuous at $\eta = 1$ when (45) and (44) are used. In contrast, the original Wilkens formulas (43) and (44) give a continuous derivative $\mathrm{d}f/\mathrm{d}\eta$ at $\eta = 1$ and can be applied to describe the asymptotic scattering.

Kaganer *et al.* (2005) proposed a simple interpolation formula for the whole range of η,

$$f(\eta) = -\ln\frac{\eta/\eta_0}{1 + \eta/\eta_0}. \qquad (46)$$

This function with $\eta_0 = 2.2$ is plotted in Fig. 8(*a*) by the dotted line. The deviation from the Wilkens curve is subtle. The diffraction peaks calculated with the function (46) are shown in Figs. 8(*b*) and 8(*c*) also by dotted lines. The deviations from the Wilkens curves are also subtle. Hence, the simple formula (46) can be used instead of the bulky formulas (43) and (44)

with the same accuracy. It also stresses the meaning of the function $f(\eta)$ in (42): it is just an appropriate interpolation function that behaves as $-\ln(gbx)$ at $x \to 0$, remains positive on $(0, \infty)$ and tends to zero at $x \to \infty$. The constant η_0 can be absorbed in the definition of the cutoff radius. These properties explain the choice of the correlation function (36).

KKS has been supported by the DFG (Grant KA 3262/1-1), RFBR (09-01-00152 and 09-01-12028-ofi-m) and a joint BMBF–FASIE Grant 7326.

References

Berkum, J. G. M. van (1994). PhD thesis, Delft University of Technology, The Netherlands.

Borbély, A., Driver, J. H. & Ungár, T. (2000). *Acta Mater.* **48**, 2005–2016.

Csikor, F. F. & Groma, I. (2004). *Phys. Rev. B*, **70**, 064106.

Garabagh, M. R. M., Nedjad, S. H., Shirazi, H., Mobarekeh, M. I. & Ahmadabadi, M. N. (2008). *Thin Solid Films*, **516**, 8117–8124.

Groma, I. (1998). *Phys. Rev. B*, **57**, 7535–7542.

Groma, I. & Monnet, G. (2002). *J. Appl. Cryst.* **35**, 589–593.

Groma, I. & Székely, F. (2000). *J. Appl. Cryst.* **33**, 1329–1334.

Groma, I., Ungár, T. & Wilkens, M. (1988). *J. Appl. Cryst.* **21**, 47–54.

Kaganer, V. M., Brandt, O., Riechert, H. & Sabelfeld, K. K. (2009). *Phys. Rev. B*, **80**, 033306.

Kaganer, V. M., Brandt, O., Trampert, A. & Ploog, K. H. (2005). *Phys. Rev. B*, **72**, 045423.

Kaganer, V. M., Köhler, R., Schmidbauer, M., Opitz, R. & Jenichen, B. (1997). *Phys. Rev. B*, **55**, 1793–1810.

Kaganer, V. M. & Sabelfeld, K. K. (2009). *Phys. Rev. B*, **80**, 184105.

Kaganer, V. M., Shalimov, A., Bak-Misiuk, J. & Ploog, K. H. (2006). *J. Phys. Condens. Matter*, **18**, 5047–5055.

Kamminga, J.-D. & Delhez, R. (2000). *J. Appl. Cryst.* **33**, 1122–1127.

Krivoglaz, M. A. (1961). *Fiz. Met. Metalloved.* **12**, 465–475.

Krivoglaz, M. A. (1996). *X-ray and Neutron Diffraction in Nonideal Crystals.* Berlin: Springer.

Krivoglaz, M. A., Martynenko, O. V. & Ryboshapka, K. P. (1983). *Fiz. Met. Metalloved.* **55**, 5–17.

Krivoglaz, M. A. & Ryboshapka, K. P. (1963). *Fiz. Met. Metalloved.* **15**, 18–31.

Kužel, R. (2007). *Z. Kristallogr.* **222**, 136–149.

Levine, L. E. & Thomson, R. (1997). *Acta Cryst.* A**53**, 590–602.

Martinez-Garcia, J., Leoni, M. & Scardi, P. (2009). *Acta Cryst.* A**65**, 109–119.

Pototskaya, V. V. & Ryboshapka, K. P. (1968). *Defects and Properties of Crystal Structures of Metals and Alloys*, pp. 97–109. Kiev: Naukova Dumka. (In Russian.)

Scardi, P. & Leoni, M. (2002). *Acta Cryst.* A**58**, 190–200.

Ungár, T., Groma, I. & Wilkens, M. (1989). *J. Appl. Cryst.* **22**, 26–34.

Ungár, T., Gubicza, J., Ribárik, G. & Borbély, A. (2001). *J. Appl. Cryst.* **34**, 298–310.

Ungar, T., Mughrabi, H., Rönnpagel, D. & Wilkens, M. (1984). *Acta Metall.* **32**, 333–342.

Warren, B. E. (1969). *X-ray Diffraction.* Reading: Addison-Wesley.

Wilkens, M. (1969). *Acta Metall.* **17**, 1155–1159.

Wilkens, M. (1970*a*). *Phys. Status Solidi A*, **2**, 359–370.

Wilkens, M. (1970*b*). *Fundamental Aspects of Dislocation Theory*, edited by J. A. Simmons, R. de Wit & R. Bullough, pp. 1195–1221. Washington: US National Bureau of Standards.

Wilkens, M. (1976). *Krist. Technik*, **11**, 1159–1169.

Zaiser, M., Miguel, M.-C. & Groma, I. (2001). *Phys. Rev. B*, **64**, 224102.